

Transient-doped organic electrochemical transistors working in current-enhancing mode as sensing devices for low concentration of oxygen dissolved in solution

Cite as: APL Mater. 8, 091103 (2020); doi: 10.1063/5.0015232

Submitted: 26 May 2020 • Accepted: 14 August 2020 •

Published Online: 1 September 2020








View Online



Export Citation



CrossMark

Francesco Decataldo,^{1,a)}  Isacco Gualandi,^{2,a)}  Marta Tassarolo,¹  Erika Scavetta,² 
and Beatrice Fraboni¹ 

AFFILIATIONS

¹Department of Physics and Astronomy, University of Bologna, Viale Bertini Pichat 6/2, 40127 Bologna, Italy

²Department of Industrial Chemistry, University of Bologna, Viale Risorgimento 4, 40136 Bologna, Italy

Note: This paper is part of the Special Topic on Advances in Bioelectronics.

a) Authors to whom correspondence should be addressed: francesco.decataldo2@unibo.it and isacco.gualandi2@unibo.it

ABSTRACT

Dissolved oxygen in cell culture media represents an interesting parameter worth monitoring, especially at very low concentrations. Indeed, cells grow faster and live longer in hypoxic conditions, and recent studies relate stronger tumor malignancy, recurrence, and progression with reduced oxygen levels. Standard techniques for dissolved oxygen evaluation rely either on optical investigations or on electrochemical methods. The former requires complex protocols and expensive instrumentations, while for the latter, the presence of a silver/silver chloride electrode hinders the device miniaturization and induces cytotoxic effects. In this work, poly(3,4-ethylenedioxythiophene):poly(styrenesulfonic acid) (Pedot:Pss)-based Organic Electrochemical Transistors (OECTs) are presented as dissolved oxygen sensors. The catalytic activity of the Pedot chains is exploited for the transduction since oxygen reduction reactions, occurring at the polymer/electrolyte interface, induce Pedot:Pss to switch from the less conductive neutral state (off) to the more conductive oxidized one (on). This transient-doping effect enhances OECT current output, which presents a high signal to noise ratio (i.e., $>10^2$ – 10^3). The transistor architecture allows for high output/input signal power amplification (i.e., >15 dB– 22 dB) and excellent sensitivities [328 ± 11 mV/dec and -0.38 ± 0.02 mA/dec for transfer and $I_{ds}(t)$, respectively], together with a low detection limit ($0.9 \mu\text{M}$, which represents the 0.07% of oxygen partial pressure). Finally, the here reported OECT sensors are demonstrated to work also in a real-life complex biological environment. This work paves the way for reliable, real-time oxygen monitoring in *in vitro* cell cultures for various relevant applications, such as investigating the influence of hypoxia conditions on cell lines or tumors.

© 2020 Author(s). All article content, except where otherwise noted, is licensed under a Creative Commons Attribution (CC BY) license (<http://creativecommons.org/licenses/by/4.0/>). <https://doi.org/10.1063/5.0015232>

INTRODUCTION

The detection of oxygen dissolved (DO) in aqueous solution is interesting in industrial, environmental, and biological fields, being related to food freshness, water quality, and cellular bio-processes, respectively.^{1,2} Regarding the latter, aerobic organisms employ oxygen to respire; thus cell metabolism, proliferation, and differentiation all involve oxygen consumption.¹

Low oxygen concentration (hypoxia) may have several consequences on cells or tissues. As an example, cells that are grown in low oxygen concentration (i.e., 3% O₂, instead of the standard environmental 20%), or even under hypoxia conditions, grow faster and live longer, showing less DNA damage, with fewer stress responses.³ Moreover, oxygen content can be used to evaluate tumor invasiveness and aggressiveness: Evans *et al.* demonstrated that increased hypoxic levels are correlated with faster tumor recurrence since

grade 2, 3, and 4 tumors showed modest (2.5% O₂), moderate (0.5% O₂), and severe (0.1% O₂) hypoxia levels, respectively;⁴ Vaupeel reported that hypoxia conditions increased tumor malignancy, leading to cells with more aggressive phenotype, promoting local and distant spread and leading to faster tumor progression (explained as an attempt of the tumoral cells to fight the hostile conditions).⁵ A reliable oxygen monitoring would be of extreme importance for a better understanding of such processes, paving the way for effective therapy development.

For DO sensing, either optical or electrochemical methods are used. The former mainly rely on the use of fluorophores⁶ or phosphorescent probes,⁷ using a plate reader for the measurements. Gold-standards in this procedure include the XF Series from Agilent, Inc. (i.e., MitoXPress⁸): even though these systems allow for monitoring intracellular and in-culture oxygen concentrations, they are based on complex and costly protocols and equipment since they require overnight incubation of the phosphorescent probes and a microplate reader for the measurements, able to maintain the cell culture environmental conditions constant. Regarding the electrochemical analysis, the most popular and reliable method is the Clark electrode (a commercial example is the Oxgraph from Hansteh, Inc.⁹), which consists of a two-electrode amperometric sensor composed of an Ag/AgCl reference electrode (RE) and a Pt working electrode (WE) soaked in a KCl solution. An O₂ permeable membrane is placed between the electrolyte and the sample to avoid interferences. When a reduction potential is applied to the WE, oxygen reduction occurs leading to an electrical current, which can be correlated with the DO concentration. A similar technique was used by Han *et al.*,¹⁰ substituting the liquid electrolyte (which may undergo evaporation) with a Nafion film as a solid, oxygen-permeable polymer electrolyte. The sensors were then compared with the XF-24 of Agilent, Inc., showing that they were able to measure cellular respiration even with fewer cells than the XF-24. However, the presence of a reference electrode often hinders the device miniaturization as screen printed silver/silver chloride reference electrodes showed poor stability.¹¹

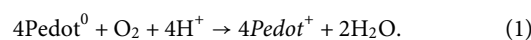
In this work, a viable and powerful alternative for dissolved oxygen detection and quantification is investigated, using Organic Electrochemical Transistors (OECTs), made with the semiconducting polymer poly(3,4-ethylenedioxythiophene):poly(styrenesulfonic acid) (Pedot:Pss). OECTs are composed of a semiconducting polymer channel and a gate electrode: both elements are soaked in the same electrolytic solution. The electronic readout of the channel can be modulated upon the application of positive/negative gate potentials, pushing/pulling positive ions inside/from the channel, changing the conductivity of the Pedot:Pss.

Pedot-based OECTs have been employed to detect several analytes, exploiting their inherent signal amplification and ease of functionalization,^{12–16} as well as for cell tissue integrity^{17–19} and toxicity evaluation,²⁰ owing to their biocompatibility and stability in the aqueous environment. In particular, our group showed that compounds undergoing redox reactions can be monitored with unfunctionalized Pedot:Pss-based OECTs, mainly focusing on reducing agents such as dopamine, adrenaline, ascorbic acid, and uric acid.^{21,22} As reported in the literature mainstream, these sensors work in depletion mode, and the analytes are detected throughout a decrease in the drain current (I_d). For low analyte concentrations, I_d slightly changes with respect to its background value, which is

very high (i.e., mA for millimeter-sized devices) since the transistor is working in its “on” state. Therefore, reaching high sensing performances is linked to the ability of performing a precise and accurate measurement of a small current variation (i.e., μA) with respect to a larger background.

On the other hand, when the devices are operated close to the threshold voltage in current-enhancing mode, I_d can increase with respect to the current value of the transistor working in the “off” state (μA variations over a μA background), thus achieving better performances, with a higher signal-to-noise ratio. Moreover, the power adsorption is very low because of small currents flowing in the channel when no analyte is present. In the first proof of concept of a sensor based on OECT, Wrighton’s group proposed the detection of oxidant species with the “off” state device, employing the *p*-type semiconductor Poly(3-methylthiophene).²³ However, such an OECT architecture needed a potentiostat endowed with a reference and a counter electrode, with some disadvantages with respect to the more modern configuration. Alternative materials have been investigated to fabricate OECTs that can work with a turned “off” device in the modern architecture, based either on *n*-type semiconductors²⁴ or *p*-type ones.²⁵ However, such new materials still present drawbacks and are in early stage development. Thus, more efforts should be directed toward commercially available products, such as the *p*-type Pedot:Pss, which guarantees superior performances in terms of conductivity and stability, owing to the research improvement of the last decade. Embracing this intention, Keene *et al.* employed aliphatic amine molecules to chemically de-dope Pedot:Pss channels in OECTs, reducing the threshold voltage values.²⁶ Even though the strategy looks promising toward enhancement-mode OECTs, the best performing transistor still presents halved hole mobility and slightly reduced normalized peak transconductances, compared to standard Pedot:Pss ones, and their sensing features are not investigated in the work.

In this work, we report how to efficiently detect an oxidant agent with an all-PEDOT OECT without the need of functionalization or molecular units. When the OECT is turned off using a positive gate bias, holes injected in the semiconducting polymer channel by an oxidizing species (transient doping) enhance the current signal. Oxygen is an example of oxidizing agents, due to its ability to accept electrons: Singh *et al.* proved, through the application of the density functional theory, that Pedot chains have the catalytic activity, allowing for oxygen reduction reaction (without the need of external dopants or platinum catalyst to facilitate the electrocatalysis) with the formation of polaronic states, which reduces the HOMO–LUMO gap.²⁷ The energetically favourable reaction proposed in the model was the following:



According to the reaction above, oxygen presence will induce Pedot:Pss to switch from the less conductive neutral state (off state) to the more conductive oxidized one, increasing the polymer conductivity, thus allowing for oxygen detection. It is worth noting that the literature reports that O₂ reduction at PEDOT:PSS could also produce hydrogen peroxide, which could have a toxic effect on cells.²⁸

The here reported transient-doped Pedot:Pss OECT working in current-enhancing mode proved to be efficient sensors for low-concentration DO monitoring, having high sensitivities, low detection limits, and high signal to noise (S/N) values. Preliminary tests, using a cell culture medium as electrolyte for the device, proved our sensors to be able to detect oxygen concentrations relevant for hypoxic biological environment. Our results pave the way for *in vitro*, real-time monitoring of cell metabolic processes in low-concentration DO, foreseeing innovative investigations on cells or tissues under hypoxia conditions.

MATERIALS AND METHODS

Device fabrication

Glass substrates were cleaned by sonication in distilled water/acetone/isopropanol baths. Afterward, 10 nm of chrome and 50 nm of gold were deposited by thermal evaporation in order to realize the contact pads and conductive tracks of the device. After that, the Pedot:Pss solution was spin coated (700 rpm for 10 s) to realize the device channel and gate electrodes using a Teflon mask. The thin film thickness is 390 ± 30 nm. The solution was made of 93.75% Pedot:Pss (Heraeus, Clevios PH1000) with 5% of ethylene glycol (EG) (Sigma Aldrich), 1% of 3-glycidoxypropyltrimethoxysilane (GOPS), and 0.25% of

4-dodecylbenzenesulfonicacid (DBSA). This suspension was treated in ultrasonic bath for 10 min and filtered through $1.2 \mu\text{m}$ cellulose acetate filters (Sartorius) before the deposition. The samples were subsequently baked at 120°C for 30 min. The resulting OECTs were patterned to have channel length (L) and width (W) of 10 mm and 3 mm, respectively, and the gate electrode with $L = 19$ mm and $W = 8$ mm. Then, devices are merged in distilled H_2O for 1 h and dried with a nitrogen flux. The final device geometry is reported in Fig. 1(a).

Biological culture medium

Dulbecco's Modified Eagle Medium (DMEM) (4.5 g l^{-1} glucose) was supplemented by 10% (v/v) fetal bovine serum (FBS), $2 \times 10^{-3} \text{ M}$ L-glutamine, 100 U ml^{-1} penicillin, and 100 mg ml^{-1} streptomycin, and 0.1 mM MEM Non Essential Amino Acids (NEAAs). The resulting solution mimicked the biological environment of a real *in vitro* cell culture, used as electrolyte.

Winkler titration

The procedure was carried out by avoiding the contamination of the sample with atmospheric O_2 , using the appropriate glassware and deaerated reagent solutions. 2 ml of a solution containing 2.15 M MnSO_4 and 2 ml of a solution containing 12.5 M NaOH , 0.9 KI , and

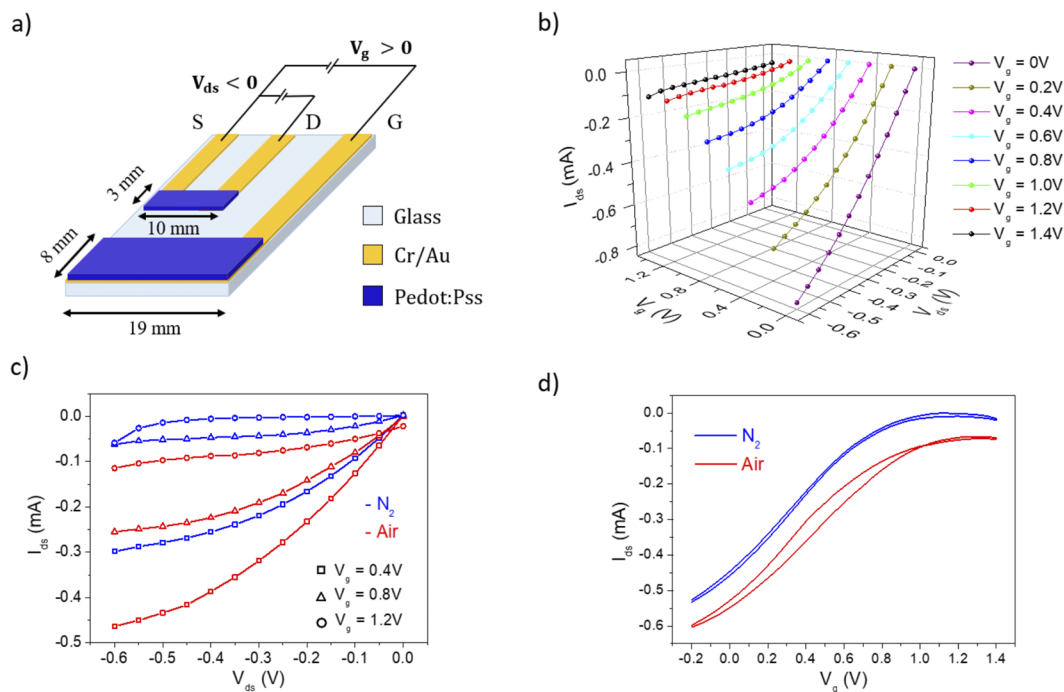


FIG. 1. (a) OECT device schematic with channel and area dimensions and the circuit electrical connections. (b) OECT characteristic curves obtained in air atmosphere, using 0.1 M KCl as electrolyte and applying a sweeping potential on the channel from 0 V to -0.6 V , for fixed V_g values (namely, 0 V , 0.2 V , 0.4 V , 0.6 V , 0.8 V , 1 V , 1.2 V , 1.4 V). (c) Output curve comparison, using 0.1 M KCl as electrolyte, in air (red line) and nitrogen-saturated (blue line) conditions (solution and atmosphere) for $V_g = 0.4 \text{ V}$ (squares), 0.8 V (triangles), and 1.2 V (circles). (d) Transfer comparison, using 0.1 M KCl as electrolyte, in air (red line) and nitrogen-saturated (blue line) conditions, sweeping V_g in the range between -0.2 V and 1.4 V , with fixed $V_{ds} = -0.3 \text{ V}$.

0.15M NaN_3 were added to 25.00 ml of the electrolyte. The mixture was stirred, and the formation of a precipitate occurred. After decanting the suspension, 2 ml of concentrated H_2SO_4 was added, and the sample was again stirred. The reaction of the reagents with O_2 leads to the formation of a stoichiometric I_2 amount, which was titrated with 0.0025M $\text{S}_2\text{O}_3^{2-}$ using a starch indicator.²⁹

Electrical characterization

Electrical data for the output, transfer, and $I_{\text{ds}}(t)$ measures were carried out employing a Keysight B2912A, used to bias the channel and gate of the devices. The OECTs were immersed in a solution of 25 ml of 0.1M KCl or DMEM for the measurements in the standard electrolyte and in the biological environment, respectively.

Electrochemical characterization

Electrochemical measurements were performed with the Metrohm Autolab Potentiostat in a three-electrode cell. An Au/Pedot:Pss electrode, having an area of 152 mm^2 (i.e., the gate electrode of an OECT), was used as the working electrode, while an Au wire and an Ag/AgCl glass electrode were employed as counter and reference electrodes, respectively.

Data analysis

The sensitivity of the sensor was extracted as the slope of the linear fit in the range under study. The calibration line was obtained by means of the linear fit of the I_{ds} vs $\log C$. The limit of detection (LOD) was calculated as the concentration that would generate a signal equal to blank signal (I_{off}), determined under N_2 atmosphere, plus three times blank standard deviation (σ). The resulting equations for $I_{\text{ds}}(t)$ are

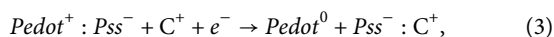
$$L.O.D.(M) = 10^{((I_{\text{off}}+3\sigma)-q)/m}, \quad (2)$$

where q and m are the intercept and the slope of the calibration line, respectively. The same equations hold for the LOD calculations on the transfer analysis, replacing I_{off} with $V_{\text{t-off}}$.

RESULTS AND DISCUSSION

OECT working principle

OECTs were realized with the planar geometry shown in Fig. 1(a), having both the gate and channel in Pedot:Pss and patterned on the same substrate. The gate area is larger than the channel one to enhance the potential drop as we hypothesize the oxygen reaction occurring at the OECT channel. The output characteristic curves were recorded in aerated 0.1M KCl solution as the electrolyte by sweeping the electrical polarization on the drain (V_{d}) from 0 V to -0.6 V for different V_{g} applied. The 3D graph in Fig. 1(b) shows how an increasing positive gate voltage reduces the device current by enhancing the number of cations injected in the semiconducting polymer channel. The following reaction explains the process:



where C^+ are the cations injected in the polymeric film, upon which Pedot switches from the oxidized (“on”) to the neutral (“off”) state.

A nearly straight line is reported for $V_{\text{g}} = 0$ V since almost no channel current modulation is obtained with a zero bias on the gate (violet dotted curve). Conversely, the highest potential of 1.2 V clearly switches the OECT in its “off” state (black dotted curve), with current lower than 100 μA for all the negative biases applied on the channel.

OECTs operating in air and N_2

OECTs performed differently when characterized in nitrogen-saturated atmosphere and solution, as shown in Figs. 1(c) and 1(d). Figure 1(c) compares OECT output curves in standard air conditions (red lines) and in oxygen-depleted ones (blue lines), for $V_{\text{g}} = 0.4$ V (square markers), 0.8 V (triangle markers), and 1.2 V (round markers). A reduction in the output current vs O_2 depletion occurs both in air and N_2 atmosphere for all the three reported gate voltages. In particular, the highest difference is observed for $V_{\text{g}} = 0.8$ V, where the device is in the “off” state (negligible current values) for nitrogen-saturated (N_2) conditions and in the “on” state in air (I_{ds} is several hundreds of μA). A further proof was obtained investigating the transcharacteristic curves of the OECT: fixing the potential on the channel at $V_{\text{ds}} = -0.3$ V (in the middle of the previous range) and sweeping the tension on the gate from -0.2 V to 1.4 V. Transfers in air and N_2 are reported in Fig. 1(c) in red and blue lines, respectively. Again, the lower current value is evident for the measure without oxygen, with a shift of the data for all the given V_{g} . Furthermore, it can be noted that the device is able to turn off only when oxygen is depleted from the solution and the above atmosphere, with an average value of the $I_{\text{off}}(\text{N}_2) = (-1.2 \pm 0.7)$ μA . Conversely, in the standard air condition, the device “off” state presents $I_{\text{off}}(\text{Air}) = (-67.0 \pm 1.1)$ μA , which is more than one order of magnitude higher compared to the one obtained in N_2 conditions. Consequently, it is evident from the transfer curves that the highest $I_{\text{on}}/I_{\text{off}}$ ratio, a key parameter for OECTs, is obtained when oxygen is not present: thus, the use of these devices as switchers would benefit a nitrogen-saturated environment.

A representative schematic of the hypothesized reaction occurring on the device, under the applied polarizations, is reported in Fig. 2(a). When V_{g} assumes high values, cations are pushed in the channel [see Eq. (3)], and the Pedot⁺ is mainly converted to Pedot⁰, with the device working in the “off” state (i.e., depleted of the holes). DO can react with the negatively polarized (vs the gate electrode) Pedot:Pss channel, switching the polymer from its neutral to its oxidized, and more conductive, state, enhancing the current flowing in the device. In the reaction, Pedot acts as an electron supplier for oxygen reduction and consequent water formation, meanwhile allowing for free hole injection from the source contact, as shown in Eq. (1) and in Fig. 2(a).

Pedot:Pss electrochemical response at different O_2 concentrations

For a better understanding of the electrochemical processes involved, a simple Au/Pedot:Pss electrode, realized with the same procedures used for the gate of the device (see the section titled Materials and Methods) was studied by means of Cyclic Voltammetry (CV) and Electrical Impedance Spectroscopy (EIS). The experimental setup used for oxygen percentage injection in the following

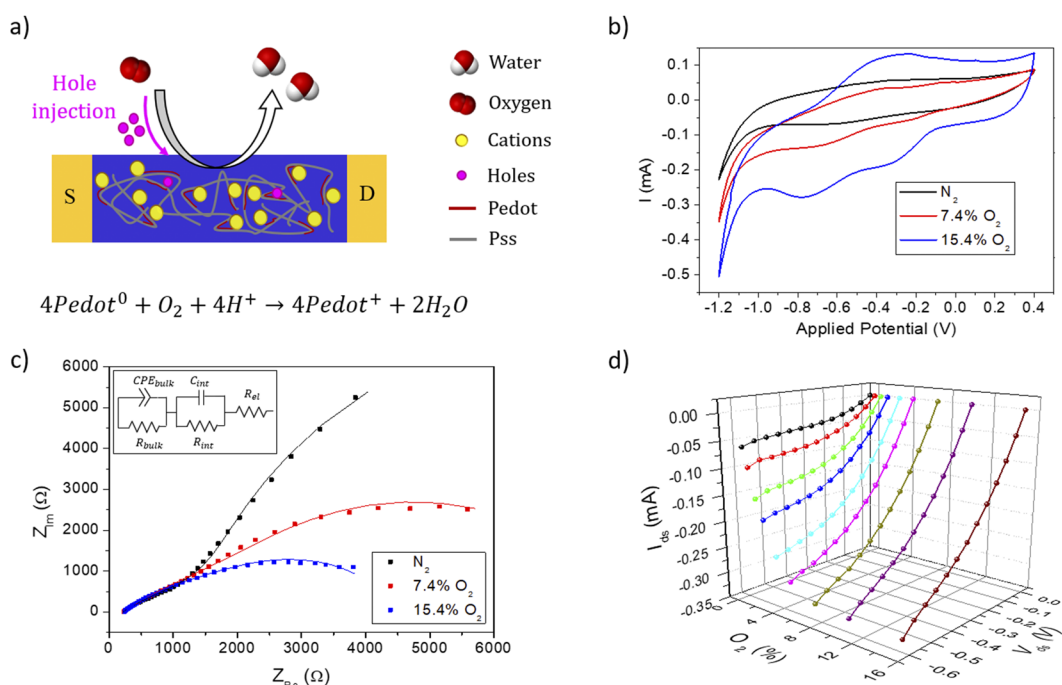


FIG. 2. (a) Schematic representation of the oxygen reduction reaction on the channel of OECTs reported in the cross section. Cyclic voltammetry (b) and electrical impedance spectroscopy (c) of an Au/Pedot:Pss electrode in 0.1M KCl for 0%, 7.36%, and 15.43% O_2 fluxed in the solution. The lines represent data fitting, according to the equivalent circuit reported in the inset. (d) Output characteristic curves of the OECT at a fixed gate voltage of 0.8 V, sweeping the channel polarization between 0 V and -0.6 V, upon different oxygen percentage introduced in the solution.

measurements is reported in Fig. S1. The oxygen concentrations in the solution were determined using the Winkler method (see the section titled Materials and Methods), and the calculated oxygen solubility constant in water ($k = 0.0013$ mol/atm l) was then used for the conversion to the oxygen partial pressure introduced. The calibration curve for the data conversion is reported in Fig. S2. CVs for nitrogen-saturated 7.4% and 15.4% O_2 amount are shown in Fig. 2(b). CV curves under nitrogen atmosphere are flat, highlighting a pseudo-capacitive response due to the processes involving Pedot:Pss [reaction in Eq. (3)]. In O_2 presence, CVs show new redox waves with peak currents linearly proportional to O_2 concentration, with a slope of -0.92 ± 0.16 A M^{-1} and R^2 of 0.895 (Fig. S3). Moreover, the reduction of hydrogen peroxide was studied on a Pedot:Pss electrode to investigate the complete reaction process (Fig. S4). The CV recorded in 0.1M KCl solution containing 1.0 mM H_2O_2 shows a redox wave with two peaks, and the onset potential of reduction is about 0 V. Since H_2O_2 reduction takes place at a less cathodic potential value than the one required for sensing reaction (< -0.2 V vs SCE), the H_2O_2 , which could be produced by O_2 , would be quickly converted to water. Such results confirm that O_2 reduction [Eq. (1)] can be considered as the reaction at the basis of signal transduction: thus, O_2 can oxidize Pedot:Pss by injecting holes in the conductive polymer, when biased below the onset potential of the process ($E < -0.1$ V vs Ag/AgCl). However, a small H_2O_2 amount could be formed from the sensing mechanism too.

Similar results are obtained for EIS spectra, extracted while applying -0.3 V to the WE. The largest differences are observed in the Nyquist plot [Fig. 2(c)], while slight changes can be found in the Bode ones [Figs. S5(a) and S5(b) for the phase and impedance, respectively]. Figure 2(c) reports the highest impedance value for N_2 -saturated conditions (black-dotted line), showing a straight line in the low frequency regime (0.1 Hz–1 Hz) that highlights a limited ion diffusion. By increasing the O_2 concentration, the impedance is reduced in this frequency range (especially lowering the imaginary value of Z, thus enhancing the capacitance of the electrode), enhancing the ion diffusion process. Accordingly, Fig. S5(a) highlights that in a N_2 -saturated environment, a capacitive behavior rules the electrode impedance for low frequency (< 1 Hz), as proven by the enhanced phase value. The equivalent circuit used to fit the experimental data is reported in the inset of Fig. 2(c), and all the characteristic parameters derived from the simulations are reported in the supplementary material (Fig. S6). It is worth to note that the interfacial resistance (R_{int}) value decreases as the oxygen percentage in solution increases, passing from 15 k Ω in the nitrogen-saturated solution (0% O_2) to 1.28 k Ω for a 15% O_2 .

OECT working at different O_2 concentrations

As explained in the work of Bernardis *et al.*,³⁰ electrochemical sensing in OECTs involves a shift of the effective gate voltage due to the presence of an additional offset voltage, dependent on the

analyte concentration, $V_g^{\text{eff}} = V_g + V_{\text{offset}}$. We obtained similar results for OECTs investigated under different oxygen concentrations with a fixed potential on the gate. Figure 2(d) underlines how the DO amount has a gating effect on the device. From a comparison of this graph with Fig. 1(b), it can be noted that an increasing oxygen concentration reduces the effective gate voltage acting on the device channel, thus introducing a negative V_{offset} , proportional to the O_2 amount. Noteworthy, also a slight introduction of oxygen in the system (i.e., 0.54% O_2) already leads to changes in the characteristic curve. Comparing Fig. 2(d) with Fig. S7, it is clearly noted that a complete current modulation in this low oxygen concentration range is achieved only for the former ($V_g = 0.8$ V). Indeed, the device is working in the “off” state for oxygen-depleted (0% O_2) conditions, showing I_{ds} values around or below $50 \mu\text{A}$, and turns “on” for oxygen amount closer to the air atmosphere, with I_{ds} reaching hundreds of μA .

Keene *et al.* observed the instability of state retention for Pedot:Pss OECTs due to the spontaneous oxidation of the Pedot:Pss channel and succeeded in reducing this process through an encapsulation of the device in an inert atmosphere.³¹ However, when OECTs are used as *in situ* sensors, an encapsulation is not possible, and the assessment of the device response and stability at different oxygen concentrations is fundamental for the calibration of

the sensing features. For example, this would be extremely important for sensors aimed at measuring analytes or other compounds close to cells, where oxygen consumption variations may lead to O_2 flux and concentration fluctuations.^{32,33}

O_2 sensing using OECTs

The I_d modulation upon oxygen percentage variations can be exploited to realize a DO sensor, especially focusing on the low-concentration O_2 detection. For this purpose, transcharacteristic measurements were carried out for different oxygen partial pressures in the range below 5% of O_2 , fixing the bias on the channel at $V_{\text{ds}} = -0.3$ V and sweeping the gate potential between -0.2 V and $+1.4$ V. The results are reported in Fig. 3(a), showing the expected current increase for raising the oxygen amount in the system.

The OECT threshold voltage (V_t) at different O_2 concentrations is reported vs the logarithm of the molar concentration of DO in the solution in Fig. 3(b). Higher O_2 concentrations shift V_t toward greater values since higher gate voltages are needed to turn off the device as the O_2 content in the electrolyte solution increases. The good linear correlation ($R^2 = 0.995$) between V_t and the logarithm of the molar concentration provides a sensitivity (S) of (328 ± 11)

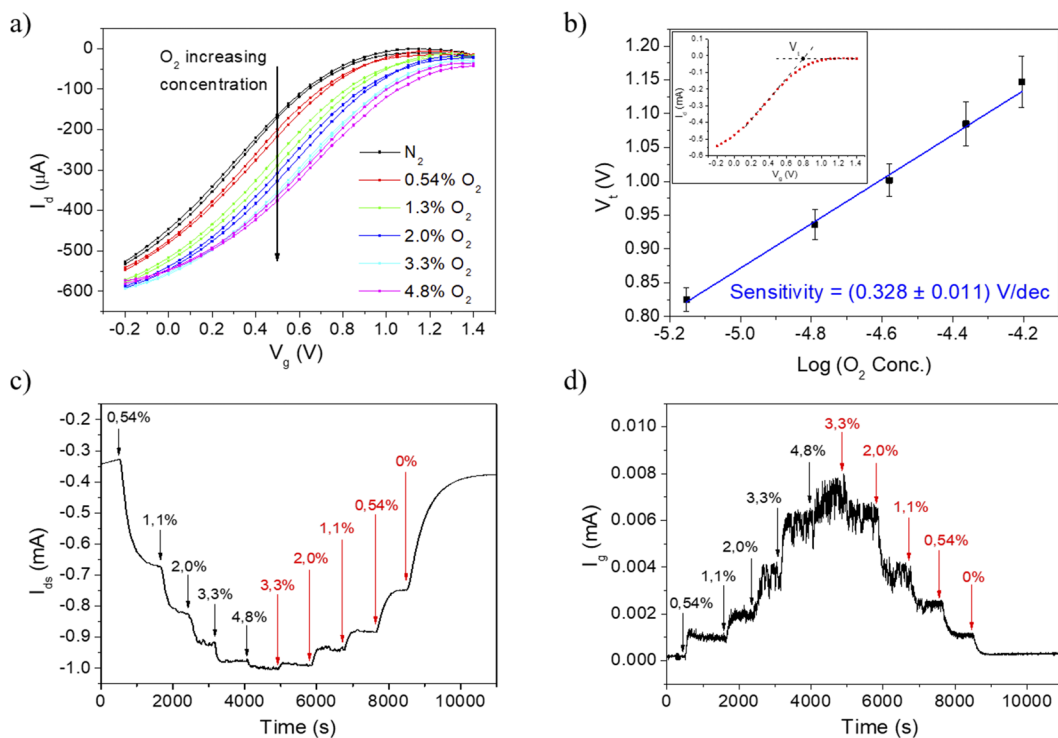


FIG. 3. OECT used as a sensor for dissolved oxygen detection, in the range below 5%, using 0.1M KCl as the electrolyte. (a) Transcharacteristic curves of the OECT for a fixed channel bias $V_{\text{ds}} = -0.3$ V, while sweeping the gate potential between -0.2 V and 1.4 V, upon different oxygen percentage in the solution. (b) Threshold voltage values obtained from the forward transfer curves in a function of the logarithm of the oxygen molar concentration. Error bars are calculated by means of error propagation. The inset represents the procedure to extract V_t , using the intersection of the straight line fitting the linear behavior of the transfer, with the horizontal line (parallel to the x axis), passing through I_{off} of the device at that oxygen concentration. (c) $I_{\text{ds}}(t)$ for oxygen addition (black arrows) and subsequent removal (red arrows) from the solution. (d) $I_g(t)$ for oxygen addition (black arrows) and subsequent removal (red arrows) from the solution.

mV/dec. Even though we are not using the sensor as a potentiometric device, this value can be roughly compared with the Nernstian response expected for a potentiometric transduction (that is around 15 mV/dec for a four electron process).³⁴ It is noteworthy that the OECT sensitivity is one order of magnitude higher, thanks to the OECT inherent amplification. The limit of detection of the OECTs is 6 μM (see the section titled Materials and Methods for the calculation), which corresponds to 0.49% of oxygen partial pressure. According to these results, V_t can be used as a quantitative parameter for oxygen sensing with OECTs.

To perform a real-time and direct evaluation of DO concentration, a potentiostatic method was employed for oxygen sensing using the same OECT, measuring the current flowing in the channel as a function of time, for fixed $V_{ds} = -0.3$ V and $V_g = +0.8$ V. The V_g was chosen after the comparison of Figs. 2(d), S7(a), and S7(b), introduced above. This value allows us to drive the device in the “off” state when oxygen is depleted, thus with negligible current flowing into the channel (i.e., low power consumption), while still leading significant current increments for oxygen increase. Figure 3(c) reports $I_{ds}(t)$ recorded for oxygen additions and subsequent removals. As expected, an increase in O_2 concentration leads to an increase in I_{ds} . Noteworthy, the oxygen depletion shows the opposite trend, with the device returning to lower currents. Even though the reported curve does not show a perfectly symmetrical trend, by plotting I_{ds} (extracted once a steady-state current was reached) as a function of the DO concentration, comparable sensitivities are obtained for the added (S_{add}) or removed (S_{rem}) oxygen amount. The linear fit values for S_{add} (-0.38 ± 0.02 mA/dec) and S_{rem} (-0.34 ± 0.04 mA/dec) are consistent and demonstrate the ability of the device to follow the addition as well as the removal of oxygen in the system. The time needed to stabilize the device after each addition is related to the time required for O_2 to completely dissolve and reach the expected constant value in the solution (usually a constant flux with a selected O_2/N_2 ratio was kept for more than 12 min–15 min to avoid possible altered oxygen concentration). We also calculated the limit of detection for this potentiostatic sensing method, obtaining a value of 0.9 μM , which represents the 0.07% of oxygen partial pressure. We report in Fig. S8 three repeated measurements over the same sensor for oxygen addition, highlighting the good repeatability, assuming a normal distribution with the weighted average value of sensitivity resulting in -0.40 ± 0.02 mA/dec.

To evaluate our device amplification features, we investigated the low current flowing between the gate and the source of the device (I_g). The oxygen reduction occurring at the channel of the device must be associated with an oxidation at the gate electrode that is measured by an I_g enhancement, which closes the electrical circuit. Since we hypothesized that a slight Pedot:Pss overoxidation is taking place at the gate electrode, we fabricated devices with a large gate area in order to keep transistor sensing performances stable over time. Figure 3(d) shows that increasing oxygen concentrations would raise the gate current (I_g) value, while lowering down the oxygen amount would lead to a current reduction. I_g is indeed correlated through the Faraday law to the rates of both oxygen reduction and holes injection in the channel. The graph shows a symmetrical consistent response, having I_g sensitivities of S_{g_add} of 0.0046 ± 0.0010 mA/dec and S_{g_rem} of 0.0048 ± 0.0007 mA/dec, though with high current fluctuations (noise) for each oxygen concentration. The comparison between I_{ds} and I_g clearly highlights the

increase of almost two order of magnitude of the sensitivity for the former, by means of the transistor architecture. Furthermore, focusing on small oxygen concentration (for example, the first addition of 0.54% O_2), it can be noted that an amplification of 22 dB is obtained between the input signal power ($\Delta I_g \times V_g$) and the output signal power ($\Delta I_{ds} \times V_{ds}$), again confirming the high amplification of the device response (signal) even for low oxygen variations.

Another consideration can be done from the comparison of $I_g(t)$ and $I_{ds}(t)$: we achieve higher signal to noise ratios for I_{ds} , compared to the highly noisy gate current. Indeed, S/N values for I_{ds} ($S/N > 10^2$ – 10^3) were always found to be at least one order of magnitude bigger than for I_g (S/N ranging from 10 to 20). As an example, the extracted S/N for the oxygen addition of 3.34% were 1089 and 18 for the channel and gate current, respectively. As a matter of fact, the OECT architecture allows for a filtering of the noise incoming from the gate current: the higher time response of these devices compared to standard inorganic MOSFETs (due to higher capacitance in the ionic circuit than the parasitic capacitance in the inorganic electronic one) reduces the bandwidth of the organic transistor, which acts as a low-pass filter. According to this finding, high frequency noises acquired in the I_g signal, eventually coming from side oxidation/reduction processes, gate current fluctuations, mechanical stirring, or external electromagnetic fields, are excluded in I_{ds} values. This filtering capability of the OECT employed as the sensor, that recalls neuromorphic properties previously demonstrated by Gkoupidenis *et al.*,³⁵ will be the subject of further investigations in following works.

Finally, we compared the normalized drain (I_{d_N}) and gate (I_{g_N}) currents to investigate the amplification of the sensing abilities of the device (Fig. S9). I_{g_N} shows higher modulation for the same oxygen additions, which was expected due to the negligible gate current value for oxygen-depleted solution. However, it presents a highly noisy signal, thus highlighting the importance of the filtering abilities of the OECT on I_d . In the end, we focused on the amplification of the device over the standard I_d current that is the bare parameter extracted and employed for oxygen quantification.

It is worthy to recall that the detection of oxidant species takes advantage of the hole injection in the semiconducting polymer; thus, the transistor can work in the “off” state while accumulating charge carriers, i.e., working in the current-enhancing mode. For this reason, the percentage of I_{ds} variation can be higher than the one observed for the device operating in depletion mode since it is not limited by the I_0 value. Indeed, current modulation driven by a reducing agent cannot be higher than 100% (when the device is completely turned off), while transistors employed for the sensing oxidizing agent can undergo current enhancement above 100%. In order to clarify this statement, we introduced a comparison between current-enhancing and depletion mode Pedot:Pss-OECT, reported in Fig. S10, using oxygen and ascorbic acid as oxidizing and reducing agents examples. Due to the different reaction kinetics of the agents, a direct comparison is not possible. However, the extracted sensitivities, calculated with I_{ds} normalized to its starting value (I_{ds_N}), highlighted a sensitivity of 1.2 ± 0.2 decade⁻¹ and below 0.2 decade⁻¹, for the current-enhancing and depletion mode transistors, respectively.³⁶ Therefore, it can be noted that oxidizing agent detection may benefit a current modulation higher than 100% (here, 120% per decade), while a threshold of 100% is always present for reducing agent sensing. Finally, it is worth noting that the operative conditions reported

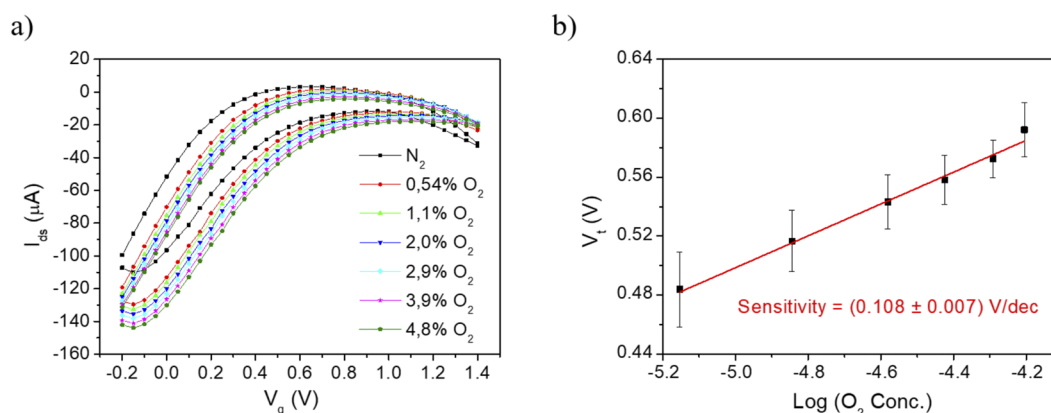


FIG. 4. Dissolved oxygen sensing in the range below 5%, using the OECT in a cell culture medium (electrolyte). (a) Transcharacteristic curves of the device for $V_{ds} = -0.3$ V, sweeping the gate potential between -0.2 V and 1.4 V, upon different oxygen percentage in the solution. (b) Threshold voltage extracted from the forward transfer curves in function of the logarithm of the oxygen molar concentration. Error bars are calculated by means of error propagation.

in this work have been chosen to enhance the I_{ds} variation and not the $I_{ds,N}$ sensitivities.

O₂ sensing in culture medium

We focused on the possible application of the here presented OECT sensors for DO monitoring in a real-life biological environment. Dulbecco Modified Eagle Medium (DMEM) was prepared to mimic a standard *in vitro* cell culture medium, having all the additives and nutrients needed for a cell growth. Due to the presence of surfactants, bubbling the nitrogen–oxygen mixture in the solution leads to formation of stable bubbles, introducing strong noises during the measurements and compromising (wetting) the contacts. Only transfer curves were then taken, introducing the device in the previously bubbled solution, then keeping a fixed oxygen–nitrogen (x%–y%) saturated atmosphere [Fig. 4(a)]. The differences between the curves recorded at different O₂ concentration are less significant in this complex electrolyte with higher ionic strength. Nonetheless, V_t values can be extracted and plotted as a function of the logarithm of the oxygen molar concentration. A linear correlation ($R^2 = 0.982$) between these two variables is again observed, obtaining a sensitivity of 108 ± 7 mV/dec. Even though the sensitivity was lower than the one achieved by the device in 0.1M KCl and V_t values have higher error bars, the resulting sensitivity still threefold exceeds the potentiometric Nernstian limit.

These results prove the ability of the here presented OECT sensors to detect oxygen dissolved in a complex biological medium, thus being able to investigate cell cultures, grown in low-concentration O₂ conditions.

CONCLUSIONS

Dissolved oxygen detection is an interesting target in several fields, especially concerning the monitoring of biological processes or cell culture, under low O₂ concentrations. Our work proves the ability of Pedot:Pss-based organic electrochemical transistors to act as high sensitivity sensors for oxygen dissolved in an electrolyte

solution. The transient-doping effect of oxygen on the polymeric material (driving Pedot to switch from its neutral state, less conductive, to the oxidized one, more conductive) induce a gating effect for the OECT that is thus working in the current-enhancing mode: positive gate potentials were used to turn off the device in nitrogen-saturated conditions (0% O₂), while increasing oxygen amounts were used to increase the current flowing in the device. Two different methods were employed to detect oxygen in 0.1M KCl: (i) the investigations of the threshold voltage shift of the transcharacteristic curves of the device and (ii) the purely amperometric current-vs-time evaluation (potentiostatic) for different oxygen amounts. High sensitivities of (328 ± 11) mV/dec and (-0.38 ± 0.02) mA/dec, together with low limit of detections of $6 \mu\text{M}$ (i.e., 0.49%) and $0.9 \mu\text{M}$ (i.e., 0.07%), for the transfer and $I_{ds}(t)$, respectively, were reported for our devices. Further improvements optimizing the device geometry will be investigated in future works. Similarly to standard OECTs working in accumulation mode, our devices present elevated S/N ratio (higher than 10^2 – 10^3), low power consumption for small oxygen concentrations, and larger I_{ds} percentual variations (>100%) compared to OECTs operated in depletion mode (~20%). Importantly, tests were performed also in a culture medium, mimicking *in vitro* cell culture experiment and demonstrating the capability of the device to sense low O₂ concentration in a complex biological environment.

The reported results pave the way to innovative and unprecedented applications, such as oxygen monitoring in cell culture grown under hypoxia conditions or the investigation of the correlation between oxygen content in the surrounding tissues and tumor aggressiveness. Scaling down the dimension of the device and implementing them in an integrated system for cell culture and electrical data acquisition would allow a non-invasive, real-time, *in situ* oxygen monitoring inside the incubator.

SUPPLEMENTARY MATERIAL

See the [supplementary material](#) for further explanations and results on our work.

AUTHORS' CONTRIBUTIONS

F.D. helped in investigation, data curation, formal analysis, and writing the original draft. I.G. performed conceptualization, data curation, methodology, supervision, and review and editing. M.T. performed supervision and review and editing. E.S. and B.F. performed funding acquisition, supervision, and review and editing.

ACKNOWLEDGMENTS

The authors acknowledge Professor Luca Pasquini for having provided the flowmeter instrumentation employed for oxygen concentration mixing.

The authors declare no conflict of interest.

DATA AVAILABILITY

The data that support the findings of this study are available from the corresponding author upon reasonable request.

REFERENCES

- 1 M. Yasukagawa, K. Yamada, S. Tobita, and T. Yoshihara, *J. Photochem. Photobiol., A* **383**, 111983 (2019).
- 2 Y. Tian, B. R. Shumway, and D. R. Meldrum, *Chem. Mater.* **22**, 2069 (2010).
- 3 B. M. Kay, *Am. Lab.* (2012), see <https://www.americanlaboratory.com/913-Technical-Articles/123131-Culturing-Cells-Under-Hypoxic-Conditions-for-Biologically-Relevant-Results/>.
- 4 S. M. Evans, K. D. Judy, I. Dunphy, W. T. Jenkins, W.-T. Hwang, P. T. Nelson, R. A. Lustig, K. Jenkins, D. P. Magarelli, S. M. Hahn, R. A. Collins, M. S. Grady, and C. J. Koch, "Hypoxia is important in the biology and aggression of human glioblastoma tumors," *10(24)*, 8177–8184 (2004).
- 5 P. Vaupel and M. A. Med, *Oncologist* **13**, 21 (2008).
- 6 F. Glauche, G. T. John, S. Arain, A. Knepper, A. Neubauer, D. Goelling, C. Lang, N. Violet, R. King, and P. Neubauer, *J. Lab. Autom.* **20**, 438 (2015).
- 7 J. Yang, Z. Wang, Y. Li, Q. Zhuang, and J. Gu, *Chem. Mater.* **28**, 2652 (2016).
- 8 See <https://www.agilent.com/en/product/cell-analysis/real-time-cell-metabolic-analysis/xf-assay-kits-reagents-cell-assay-media/mitoxpress-intra-intracellular-oxygen-assay-740893#howitworks> for MitoXPress technology.
- 9 See <https://www.hansatech-instruments.com/product/oxygraph-system/> for Oxgraph from Hansatech Inc.
- 10 J.-H. Han, S. Kim, J. Choi, S. Kang, Y. K. Pak, and J. J. Pak, *Sens. Actuators, B* **306**, 127465 (2020).
- 11 M. Sophocleous and J. K. Atkinson, *Sens. Actuators, A* **267**, 106 (2017).
- 12 I. Gualandi, M. Tassarolo, F. Mariani, T. Cramer, D. Tonelli, E. Scavetta, and B. Fraboni, *Sens. Actuators, B* **273**, 834 (2018).
- 13 F. Mariani, I. Gualandi, M. Tassarolo, B. Fraboni, and E. Scavetta, *ACS Appl. Mater. Interfaces* **10**, 22474 (2018).
- 14 A.-M. Pappa, V. F. Curto, M. Braendlein, X. Strakosas, M. J. Donahue, M. Fiocchi, G. G. Malliaras, and R. M. Owens, *Adv. Healthcare Mater.* **5**, 2295 (2016).
- 15 F. Decataldo, V. Druet, A.-M. Pappa, E. Tan, A. Savva, C. Pitsalidis, S. Inal, J.-S. Kim, B. Fraboni, R. M. Owens, and D. Iandolo, *Flexible Printed Electron.* **4**, 044006 (2019).
- 16 M. Braendlein, A.-M. Pappa, M. Ferro, A. Lopresti, C. Acquaviva, E. Mamessier, G. G. Malliaras, and R. M. Owens, *Adv. Mater.* **29**, 1605744 (2017).
- 17 F. Decataldo, M. Barbalinardo, M. Tassarolo, V. Vurro, M. Calienni, D. Gentili, F. Valle, M. Cavallini, and B. Fraboni, *Adv. Mater. Technol.* **4**, 1900207 (2019).
- 18 M. Ramuz, A. Hama, M. Huerta, J. Rivnay, P. Leleux, and R. M. Owens, *Adv. Mater.* **26**, 7083 (2014).
- 19 V. F. Curto, B. Marchiori, A. Hama, A.-M. Pappa, M. P. Ferro, M. Braendlein, J. Rivnay, M. Fiocchi, G. G. Malliaras, M. Ramuz, and R. M. Owens, *Microsyst. Nanoeng.* **3**, 17028 (2017).
- 20 F. Decataldo, M. Barbalinardo, D. Gentili, M. Tassarolo, M. Calienni, M. Cavallini, and B. Fraboni, *Adv. Biosyst.* **4**(1), 1900204 (2020).
- 21 I. Gualandi, D. Tonelli, F. Mariani, E. Scavetta, M. Marzocchi, and B. Fraboni, *Sci. Rep.* **6**, 35419 (2016).
- 22 I. Gualandi, M. Marzocchi, E. Scavetta, M. Calienni, A. Bonfiglio, and B. Fraboni, *J. Mater. Chem. B* **3**, 6753 (2015).
- 23 J. W. Thackeray, H. S. White, and M. S. Wrighton, *J. Phys. Chem.* **89**, 5133 (1985).
- 24 A. M. Pappa, D. Ohayon, A. Giovannitti, I. P. Maria, A. Savva, I. Uguz, J. Rivnay, I. McCulloch, R. M. Owens, and S. Inal, *Sci. Adv.* **4**, eaat0911 (2018).
- 25 S. Inal, J. Rivnay, P. Leleux, M. Ferro, M. Ramuz, J. C. Brendel, M. M. Schmidt, M. Thelakkat, and G. G. Malliaras, *Adv. Mater.* **26**, 7450 (2014).
- 26 S. T. Keene, T. P. A. Pol, D. Zakhidov, C. H. L. Weijtens, R. A. J. Janssen, A. Salleo, and Y. Burgt, *Adv. Mater.* **32**, 2000270 (2020).
- 27 S. K. Singh, X. Crispin, and I. V. Zozoulenko, *J. Phys. Chem. C* **121**, 12270 (2017).
- 28 A. Giovannitti, R. B. Rashid, Q. Thiburce, B. D. Paulsen, C. Cendra, K. Thorley, D. Moia, J. T. Mefford, D. Hanifi, D. Weiyuan, M. Moser, A. Salleo, J. Nelson, I. McCulloch, and J. Rivnay, *Adv. Mater.* **32**, 1908047 (2020).
- 29 L. W. Winkler, *Ber. Dtsch. Chem. Ges.* **21**, 2843 (1888).
- 30 D. A. Bernards, D. J. Macaya, M. Nikolou, J. A. DeFranco, S. Takamatsu, and G. G. Malliaras, *J. Mater. Chem.* **18**, 116 (2008).
- 31 S. T. Keene, A. Melianas, Y. van de Burgt, and A. Salleo, *Adv. Electron. Mater.* **5**, 1800686 (2019).
- 32 Y. Hayakawa, T. Nemoto, M. Iino, and H. Kasai, *Cell Calcium* **37**, 359 (2005).
- 33 D. M. Porterfield, R. F. Corkey, R. H. Sanger, K. Tornheim, P. J. S. Smith, and B. E. Corkey, *Diabetes* **49**, 1511 (2000).
- 34 A. Bard and L. Faulkner, *Russ. J. Electrochem.* **38**, 1505 (2002).
- 35 P. Gkoupidenis, N. Schaefer, B. Garlan, and G. G. Malliaras, *Adv. Mater.* **27**, 7176 (2015).
- 36 I. Gualandi, E. Scavetta, F. Mariani, D. Tonelli, M. Tassarolo, and B. Fraboni, *Electrochim. Acta* **268**, 476 (2018).